



# On the variability of atmospheric $^{222}\text{Rn}$ activity concentrations measured at Neumayer, coastal Antarctica

R. Weller<sup>1</sup>, I. Levin<sup>2</sup>, D. Schmithüsen<sup>2</sup>, M. Nachbar<sup>2</sup>, J. Asseng<sup>1</sup>, and D. Wagenbach<sup>2</sup>

<sup>1</sup>Alfred-Wegener-Institut Helmholtz-Zentrum für Polar- und Meeresforschung, Am Handelshafen 12, 27570 Bremerhaven, Germany

<sup>2</sup>Institut für Umweltphysik, Heidelberg University, Im Neuenheimer Feld 229, 69120 Heidelberg, Germany

Correspondence to: R. Weller (rolf.weller@awi.de)

Received: 15 November 2013 – Published in Atmos. Chem. Phys. Discuss.: 13 December 2013

Revised: 18 February 2014 – Accepted: 20 March 2014 – Published: 17 April 2014

**Abstract.** We report on continuously measured  $^{222}\text{Rn}$  activity concentrations in near-surface air at Neumayer Station in the period 1995–2011. This 17-year record showed no long-term trend and has overall mean  $\pm$  standard deviation of  $(0.019 \pm 0.012) \text{ Bq m}^{-3}$ . A distinct and persistent seasonality could be distinguished with maximum values of  $(0.028 \pm 0.013) \text{ Bq m}^{-3}$  from January to March and minimum values of  $(0.015 \pm 0.009) \text{ Bq m}^{-3}$  from May to October. Elevated  $^{222}\text{Rn}$  activity concentrations were typically associated with air mass transport from the Antarctic Plateau. Our results do not support a relation between enhanced  $^{222}\text{Rn}$  activity concentrations at Neumayer and cyclonic activity or long-range transport from South America. The impact of oceanic  $^{222}\text{Rn}$  emissions could not be properly assessed but we tentatively identified regional sea ice extent (SIE) variability as a significant driver of the annual  $^{222}\text{Rn}$  cycle.

pared to 3.82 d for  $^{222}\text{Rn}$ ) are continuously emitted into the atmosphere. Apart from local mineralogy and element composition of the soil, continental emission rates depend on soil texture and soil humidity and typically range between 0.005 and  $0.050 \text{ Bq m}^{-2} \text{ s}^{-1}$  (Nazaroff, 1992; Karstens et al., 2013), about two orders of magnitude higher than oceanic emissions (e.g. Schery and Huang, 2004). For the latter a recent study derived from long-term  $^{222}\text{Rn}$  observation at Cape Grim (Tasmania) an oceanic  $^{222}\text{Rn}$  emission rate of around  $2.7 \times 10^{-4} \text{ Bq m}^{-2} \text{ s}^{-1}$  (Zahorowski et al., 2013).

There are three main issues attracting some attention to atmospheric  $^{222}\text{Rn}$ , usually specified as activity concentrations in units of  $\text{Bq m}^{-3}$ : (i) being an  $\alpha$ -emitter,  $^{222}\text{Rn}$  is a potential health hazard, particularly in certain regions with elevated  $^{226}\text{Ra}$  occurrence and in poorly ventilated buildings built with  $^{226}\text{Ra}$  rich stonework (Nazaroff, 1992); (ii) in terms of atmospheric chemistry, ionizing radiation emanated from  $^{222}\text{Rn}$  entails ion mediated particle nucleation, preferentially within the continental planetary boundary layer (PBL; Harrison and Carslaw, 2003; Hirsikko et al., 2011; Zhang et al., 2011); there,  $^{222}\text{Rn}$  could exceed the impact of cosmic radiation on particle nucleation (Zhang et al., 2011); (iii) considering the relatively short radioactive half-life of 3.82 d combined with chemical inertness, the atmospheric and radioactive lifetimes of  $^{222}\text{Rn}$  are identical. Hence,  $^{222}\text{Rn}$  is a virtually ideal atmospheric tracer: on smaller spatial scales, turbulent vertical mixing within the troposphere (especially within the PBL) and soil emission fluxes have been assessed (Liu et al., 1984; Levin et al., 2002; Slemr et al., 2013), and on a larger, e.g. continental-scale long-range transport and air mass history could be derived from  $^{222}\text{Rn}$  measurements

## 1 Introduction

The radioactive noble gas radon, specifically the isotopes  $^{222}\text{Rn}$  and  $^{220}\text{Rn}$  are the sole gaseous progenies of the  $^{238}\text{U}$  and  $^{232}\text{Th}$  radioactive series, respectively. Both natural actinides are trace elements omnipresent in all minerals and soils (Nazaroff, 1992).  $^{222}\text{Rn}$  is a direct product of the  $\alpha$ -decay of  $^{226}\text{Ra}$  about a factor of  $10^{-4}$  less abundant in surface ocean waters compared to terrestrial soils (Wilkening and Clements, 1975) making the ocean only a minor  $^{222}\text{Rn}$  source. From these global surface sources, the gaseous decay product  $^{222}\text{Rn}$  (and to a lesser extent  $^{220}\text{Rn}$  because of its much shorter radioactive half-life time  $T_{1/2}$  of 56 s com-

(e.g. Law et al., 2010). Due to these attributes, observed atmospheric  $^{222}\text{Rn}$  activity concentrations were frequently used to validate global atmospheric circulation models (e.g. Jacob et al., 1997). Basically all these applications of atmospheric  $^{222}\text{Rn}$  activity concentrations broadly presume negligible oceanic  $^{222}\text{Rn}$  emissions. Interestingly, in a recent study long-term  $^{222}\text{Rn}$  observations from the remote station Cape Grim were employed to derive oceanic  $^{222}\text{Rn}$  emission rates by carefully screening the data set, mainly with the help of a thorough backward trajectory analysis (Zahorowski et al., 2013). In addition, Taguchi et al. (2013) assessed  $^{222}\text{Rn}$  air–sea transfer rates derived from ship-borne  $^{222}\text{Rn}$  measurements with the help of a global atmospheric transport model. Both approaches illustrated that in certain remote marine regions the impact of marine  $^{222}\text{Rn}$  emissions may be decisive. Among such regions, notably Antarctica and the surrounding Southern Ocean have to be considered, particularly with regard to the fact that the ice covered Antarctic continent is virtually free from  $^{222}\text{Rn}$  emissions. Moreover, due to the fact that air–sea exchange is highly dependent on surface wind velocity, specifically the stormy Southern Ocean could be a significant  $^{222}\text{Rn}$  source (Schery and Huang, 2004; Taguchi et al., 2013). Previous measurements from that region revealed extremely low  $^{222}\text{Rn}$  activity concentrations (Maenhaut et al., 1979; Polian et al., 1986; Pereira, 1990; Lambert et al., 1990; Wyputta, 1997; Ilić et al., 2005), which may be hypothetically consistent with recently ascertained marine emissions there (Zahorowski et al., 2013). Modelling studies by Heimann et al. (1990) predicted for instance in the case of Neumayer a contribution of oceanic  $^{222}\text{Rn}$  emissions to be around 28 % (derived from Table 2 therein). Nevertheless, data evaluation and discussion presented in previous studies implied that background  $^{222}\text{Rn}$  activity concentrations in this region were mainly determined by long-range transport from continental region, i.e. for the Atlantic sector of Antarctica dominantly from South America (Polian et al., 1986; Pereira, 1990; Lambert et al., 1990; Wyputta, 1997). Observed spikes in  $^{222}\text{Rn}$  activity concentrations, so-called radon storms frequently exceeding background activity concentrations by about an order of magnitude for several hours, were usually attributed to efficient long-range transport by cyclonic activity from South America (Polian et al., 1986; Wyputta, 1997). Apart from an only local impact of Antarctic  $^{222}\text{Rn}$  emissions from very few ice-free regions situated mainly on the Antarctic Peninsula (Pereira, 1990) but probably also in coastal dry valleys and high mountain ranges, recent investigations of Taguchi et al. (2013) suggested a perceptible contribution of these sources for the remote Southern Ocean. However, considering the extremely small all-up area of insularly distributed rocky places in continental Antarctica, this appears somewhat arguable.

In this paper we present an analysis of long-term  $^{222}\text{Rn}$  activity concentrations recorded continuously at the German Antarctic Station Neumayer (NM) from 1995 to 2011. We shall discuss the variability of this time series on differ-

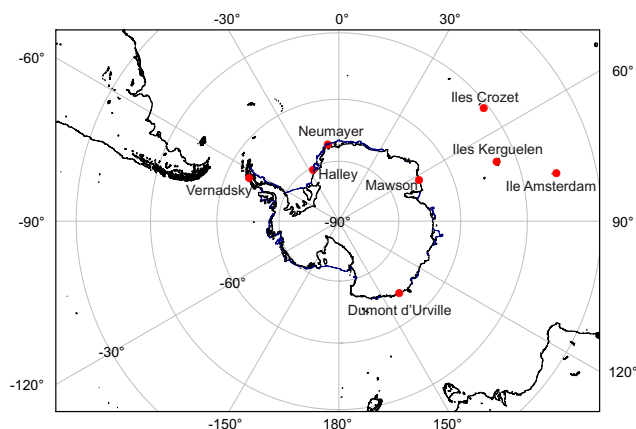


**Fig. 1.** Map of the high-latitude Southern Hemisphere showing the locations of the measuring sites discussed in the text.

ent timescales, especially focusing on its distinct seasonality. The central topic guiding us through the analysis is the question of to what extent marine, in contrast to continental,  $^{222}\text{Rn}$  emissions were responsible for the observed variability, bearing in mind that marine  $^{222}\text{Rn}$  emissions should be decisively governed by the seasonal wax and wane of sea ice. Our evaluation is further supported by local meteorological observations, backward trajectories, sea ice extent records and finally long-term  $^{210}\text{Pb}$  measurements (Elsässer et al., 2011), a  $^{222}\text{Rn}$  progeny with a half-life time of  $T_{1/2} = 22.3$  years.

## 2 Experimental techniques and data evaluation methods

### 2.1 Site description

$^{222}\text{Rn}$  measurements were conducted during the period 1995 to 2011 at the Air Chemistry Observatory, Neumayer Station ( $70^{\circ}39' \text{ S}$ ,  $8^{\circ}15' \text{ W}$ , [http://www.awi.de/en/go/air\\_chemistry\\_observatory](http://www.awi.de/en/go/air_chemistry_observatory)). A map of all relevant stations here discussed is shown in Fig. 1. Neumayer is located on an ice shelf about 10 km away from the ice shelf edge. Apart from open water or seasonal sea ice cover the surroundings are totally ice-covered and the nearest insular rocky outcrops are more than 200 km away. In several papers, the measuring site, meteorological conditions and contamination free sampling have already been described in depth and we just refer here in particular to Wagenbach et al. (1988), König-Langlo et al. (1998) and Weller et al. (2008, 2011a, b). Due to snow accumulation the observatory has to be typically jacked up every 2 years and hence the sampling height (inlet) varied between 6 and 8 m above ground.

## 2.2 Atmospheric $^{222}\text{Rn}$ activity measurements

The activity concentration of the noble gas  $^{222}\text{Rn}$  was indirectly determined by measuring the activity of the short-lived metallic daughters, namely  $^{218}\text{Po}$  ( $T_{1/2} = 3$  min) and  $^{214}\text{Po}$  ( $T_{1/2} = 162 \mu\text{s}^{-1}$ ) which are attached to sub- $\mu\text{m}$  aerosol particles immediately after generation (Porstendörfer, 1994). We used a well-established home-made  $^{222}\text{Rn}$  monitor based on the static filter method (Levin et al., 2002). In short, the basic components of this monitor comprised an adapted filter holder equipped with quartz fibre filter (Whatman QMA,  $\varnothing 47$  mm), an  $\alpha$ -detector with pre-amplifier and required data acquisition electronics. A continuously monitored flow of ambient air was pumped through the quartz filter, enabling a complete interception of all particle-bound  $^{222}\text{Rn}$  progenies. At the same time, the overlapping  $\alpha$  activity spectra of  $^{218}\text{Po}$  ( $\alpha_E = 6.0$  MeV) and  $^{214}\text{Po}$  ( $\alpha_E = 7.7$  MeV), were measured in situ with a surface barrier detector (Canberra CAM AB 900 mm<sup>2</sup> active surface, energy resolution 50 keV at 5.486 MeV). At NM, the mean  $\alpha$ -activity of the  $^{222}\text{Rn}$  daughters was determined in 3 h intervals. From the measured  $^{214}\text{Po}$  activity we then estimated the atmospheric  $^{222}\text{Rn}$  activity concentration, assuming radioactive equilibrium between  $^{222}\text{Rn}$  and its daughter  $^{214}\text{Po}$ . The overall accuracy of our  $^{222}\text{Rn}$  activity concentrations measured at NM was estimated to be about  $\pm (25\text{--}30)\%$ . This estimate includes the uncertainties of flow rate, detection noise and counting statistics as well as the potential disequilibrium between  $^{222}\text{Rn}$  and  $^{214}\text{Po}$ . For the latter, we considered the fact that disequilibrium effects were not determined at NM. The reproducibility of our measurements at NM has been determined to better than 15 % based on parallel measurements of two independent monitors over a period of more than 6 months. Continuous  $^{222}\text{Rn}$  observation started at NM in February 1983. The respective data set prior to 1995 is not included here, since the assimilation of the counts has been achieved via pre-set energy windows rather than ADC-based spectrum assay. The lower quality in the raw count data evaluation allows us to refrain from discussing the entire NM radon record, although mean  $^{222}\text{Rn}$  levels in the pre-1995 period are quite comparable to those presented here (see Wyputta, 1997).

## 2.3 Evaluation methods and auxiliary data sources

In order to study the origin of the advected air masses we rely on 10-day backward trajectories provided by the HYSPLIT 4.0 (Hybrid Single-Particle Lagrangian Integrated trajectory; [http://www.arl.noaa.gov/documents/reports/hysplit\\_user\\_guide.pdf](http://www.arl.noaa.gov/documents/reports/hysplit_user_guide.pdf)). For all trajectory calculations we used NCAR/NCEP reanalysis meteorological data with a spatial resolution of  $2.5^\circ \times 2.5^\circ$  (longitude  $\times$  latitude grid). Calculations were executed in 1-hour time steps. Due to the fact that vertical wind components in reanalysis data could be somewhat problematic especially for regions with sparse meteorological input data (like the Southern Ocean; Harris et al.,

2005), all trajectories were calculated using the 3-D wind fields of the reanalysis data as well as employing the isentropic approximation. There were significant differences between individual 10-day back trajectories calculated either under 3-D (wind vector from meteorological data) or isentropic approximation, but the general advection characteristic on which our conclusions were finally based appeared robust. More information on the accuracy of back trajectory estimates can be found in a review by Stohl (1998). Therefore we conclude that the simple backward trajectory analyses used here are appropriate for our purpose, particularly with regard to the sparse underlying meteorological data for high southern latitudes. For the same reason the validity of back trajectories exceeding 10 days appeared little conclusive due to their large spatial uncertainty.

In contrast to ice-free terrestrial surfaces, the Antarctic continent can be regarded as virtually  $^{222}\text{Rn}$  source-free, more precisely  $^{222}\text{Rn}$  emissions are restricted to a few outcropping rocks (so-called nunataks) especially on the Antarctic Peninsula, bare soil and rocky terrains at the coastal ice edge and in dry valleys. Irrespective of the fact that the surface could be a  $^{222}\text{Rn}$  source or sink (the latter for particle-bound  $^{222}\text{Rn}$  progenies), the characteristics of the boundary layer, in particular the depth of the mixing layer, co-determines the actually measured atmospheric  $^{222}\text{Rn}$  activity concentration. Surface inversions are prevalent in Antarctica extending up to about 2 km during winter while from November to February inversions are rare and confined to heights of less than 1 km (König-Langlo et al., 1998). However, for most of the time an at least moderately stable boundary layer (SBL) is present, whose thickness can be estimated as the lowest altitude above ground where the vertical heat flux ceased to a small fraction of its surface value (typically 5 %, Caughey et al., 1979). According to Handorf (1996) the SBL at NM typically ranged between 10 m and 50 m, consistent with tether sondes and sodar results from Halley Station (Anderson and Neff, 2008; Jones et al., 2010), like NM a site on the ice shelf with comparably flat surface topography. Although vertical mixing depth is not well characterized in a SBL (Anderson and Neff, 2008), we tried to gauge vertical mixing in that layer like in Weller et al. (2011a) by using the local bulk Richardson number (Stull, 1988):

$$Ri_B = \frac{g \Delta \theta / \Delta z}{\theta \left[ \left( \frac{\Delta U}{\Delta z} \right)^2 + \left( \frac{\Delta V}{\Delta z} \right)^2 \right]}, \quad (1)$$

with  $g$  the gravitational constant ( $9.81 \text{ m s}^{-2}$ ),  $z$  the height above ground,  $\theta$  the dry potential temperature, and  $U$  and  $V$  the horizontal wind vectors in  $x$  and  $y$  direction, respectively. Gradients were approximated by the difference of the measured temperatures and wind velocities at 2 m and 10 m height. Note that at least for small Richardson numbers (well below 1.0), fluxes within the SBL appear to be a continuous function of  $Ri_B$  (Fernando and Weil, 2010, Mauritsen and Svensson, 2007).

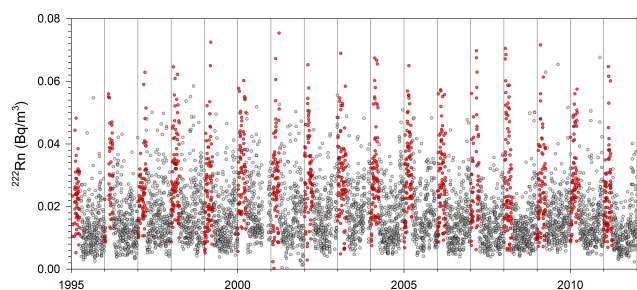


**Fig. 2.**  $^{222}\text{Rn}$  activity time series based on daily means; red circles refer to summer (JFM) values.

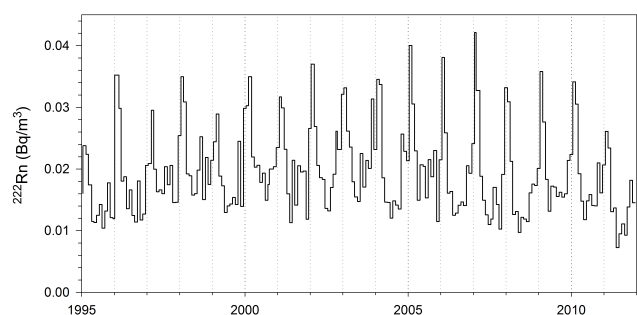


**Fig. 3.**  $^{222}\text{Rn}$  activity time series based on monthly means.

Finally we used sea ice extent (SIE; i.e. sea ice area in units  $10^6 \text{ km}^2$ ) data from the National Snow and Ice Data Center (NSIDC, <http://nsidc.org/>) with an original grid resolution of  $25 \times 25 \text{ km}^2$  until 2002 and from then on  $6.25 \times 6.25 \text{ km}^2$ . Our analysis was based on a resampled data set with a longitudinal resolution of 10 degrees (Weller et al., 2011b).

### 3 Results

#### 3.1 Data presentation

Figure 2 presents an overview of the daily mean  $^{222}\text{Rn}$  activity concentration time series continuously recorded between 1995 and 2011 at NM. In addition, monthly means of the time series are depicted in Fig. 3 (Supplement data are available at <http://doi.pangaea.de/10.1594/PANGAEA.822027>). At first glance, overall  $^{222}\text{Rn}$  levels at NM appeared constant throughout the observation period, with a long-term median of  $0.016 \text{ Bq m}^{-3}$  (mean =  $0.019 \text{ Bq m}^{-3}$ , standard deviation  $\text{SD} = 0.012 \text{ Bq m}^{-3}$ ). Indeed, a statistical trend analyses, either by simple linear regression or non-parametric rank-order Mann–Kendall test with Sen’s slope estimate (Hirsch et al., 1982), revealed no meaningful long-term trend. Nevertheless, there seems to be a broad and gentle maximum between 1998 and 2006, especially discernible in Fig. 3.

Apart from the latter rather marginal and yet unexplained finding, the salient feature is a striking seasonality with a maximum around austral summer (Fig. 4).

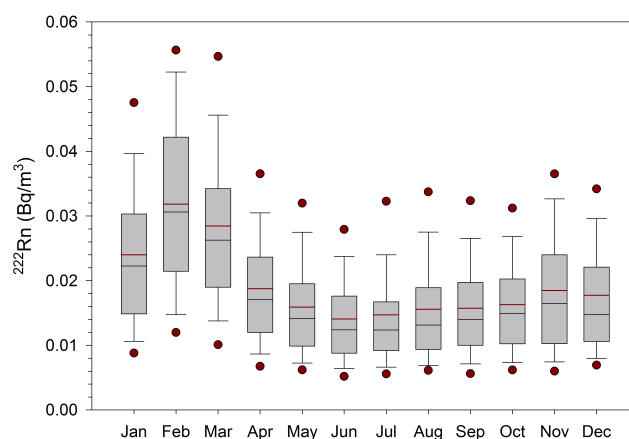


**Fig. 4.** Box plots for the mean seasonality of  $^{222}\text{Rn}$  activity observed from 1995 to 2011. Lines in the middle of the boxes represent sample medians (mean: red line), lower and upper lines of the boxes are the 25th and 75th percentiles; whiskers indicate the 10th and 90th percentiles, dots 5th and 95th percentiles.

This summer maximum appears uniformly each year between January and March with a mean  $\pm \text{SD}$  of  $(0.028 \pm 0.013) \text{ Bq m}^{-3}$  and these three months (JFM) will be henceforth defined as (local) “summer”. A broad minimum of  $(0.015 \pm 0.009) \text{ Bq m}^{-3}$  emerged from May to October (MJJASO) and this period will be termed (local) “winter” throughout the paper. Finally we address here the variability on smaller timescale and inspect to this end the  $^{222}\text{Rn}$  time series in the highest available temporal resolution (3 h bins) separately for summer and winter; however, we cannot detect any significant diurnal cycle in either case.

#### 3.2 Impact of local meteorology and long range transport

In contrast to aerosol-bound radionuclides like  $^{210}\text{Pb}$ , the sole  $^{222}\text{Rn}$  sink is radioactive decay which occurs homogeneously throughout a vertical air column while for the former a vertical gradient caused by the surface sink is typical. Taking into account that the ice shelf is definitely  $^{222}\text{Rn}$  source-free, a given  $^{222}\text{Rn}$  reservoir below a surface inversion layer should be more or less depleted by radioactive decay, provided this inversion layer is isolated from the atmosphere above. In this regard we have to consider that during summer a nocturnal inversion layer, largely preventing vertical mixing, could be frequently observed at NM. Regarding the radioactive decay time, we may barely expect a significant diurnal  $^{222}\text{Rn}$  cycle, since an even 12 h lasting surface inversion would at most cause 14 %  $^{222}\text{Rn}$  depletion. This conclusion, which is consistent with our observations, was further supported by an analysis in terms of PBL stability, assessed by bulk Richardson number  $Ri_B$  (accordingly defined as turbulent PBL for  $Ri_B < 0.25$  compared to laminar flow conditions for  $Ri_B > 1.0$ ). Concerning summer,

no significant difference ( $p = 0.9$ ) in  $^{222}\text{Rn}$  activity concentrations could be verified between both stability cases ( $0.0279 \text{ Bq m}^{-3}$  compared to  $0.0283 \text{ Bq m}^{-3}$  for laminar and turbulent conditions, respectively). The situation is different for polar night where  $^{222}\text{Rn}$  activity concentrations appeared significantly higher ( $p = 0.0002$ ) in a well-mixed, turbulent boundary layer ( $0.0157 \text{ Bq m}^{-3}$ ,  $N = 8726$ ) compared to laminar flow conditions ( $0.0135 \text{ Bq m}^{-3}$ ,  $N = 228$ ). During that period, vertical mixing should usually be much longer suppressed by persistent surface inversions, occasionally lasting for several days compared to only some hours during polar day. A more detailed inspection revealed, however, that distinct  $^{222}\text{Rn}$  depletion events are rarely observed under such lasting stagnant flow condition, indicating that an effective isolation of near-surface air masses at NM was usually not given. Nevertheless, we tentatively argue that on the whole, stagnant conditions (characterized by  $Ri_B > 1$ ) probably caused on average appreciably lower  $^{222}\text{Rn}$  activity concentrations within the SBL during winter.

In a further attempt we examined the prevalent assumption that  $^{222}\text{Rn}$ -rich air masses are efficiently advected by cyclonic activity from northerly continents (mainly South America in the case of NM) towards Antarctica (Polian et al., 1986; Pereira, 1990; Wyputta, 1997). To this end we relied on long-term meteorological observations at NM (König-Langlo et al., 1998), and categorized the general weather situation into “marine cyclonic” with high wind velocities  $> 15 \text{ m s}^{-1}$  associated with easterly wind directions within the sector  $60^\circ\text{--}120^\circ$  in contrast to “continental”, characterized by low wind velocities  $< 8 \text{ m s}^{-1}$  and southerly wind directions between  $140^\circ$  and  $200^\circ$ . Again, we examined  $^{222}\text{Rn}$  activity concentrations under these weather conditions separately for summer and winter. Contrary to our expectations, daily mean  $^{222}\text{Rn}$  activity concentrations were significantly higher ( $p < 10^{-88}$ ) under continental advection from the interior ice sheet during summer ( $0.0326 \text{ Bq m}^{-3}$ ,  $N = 5428$ , compared to  $0.0246 \text{ Bq m}^{-3}$ ,  $N = 1972$  for marine cyclonic conditions), while for winter virtually no difference was discernible ( $p = 0.5$ ;  $0.0155 \text{ Bq m}^{-3}$  compared to  $0.0150 \text{ Bq m}^{-3}$  for continental and marine cyclonic conditions, respectively).

This rather simple evaluation was further supported by more detailed trajectory analyses. First we calculated 10-day backward trajectories for days with the 10 highest mean  $^{222}\text{Rn}$  activity concentrations (so-called radon storms) trying to identify long-range transport from northward continents, especially South America. Surprisingly, the result presented in Fig. 5 did not show any “radon storm trajectory” originating from South America or any other northern continent. In a next attempt, the same procedure was done for the 10 lowest daily  $^{222}\text{Rn}$  activity concentrations (Fig. 6). In contrast to highest  $^{222}\text{Rn}$  events, lowest values could be observed throughout the year without a distinct seasonal preference. In conclusion, neither the highest nor the lowest observed  $^{222}\text{Rn}$  activity concentrations were linked with

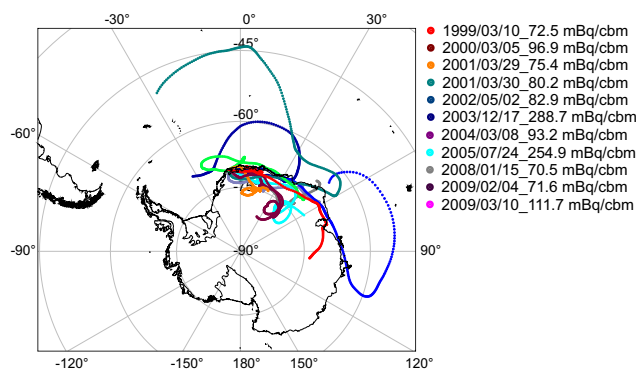


Fig. 5. The 10-day back trajectories for highest  $^{222}\text{Rn}$  activity concentrations.

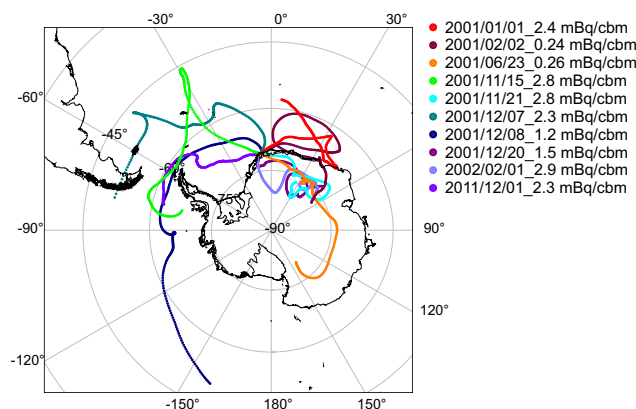
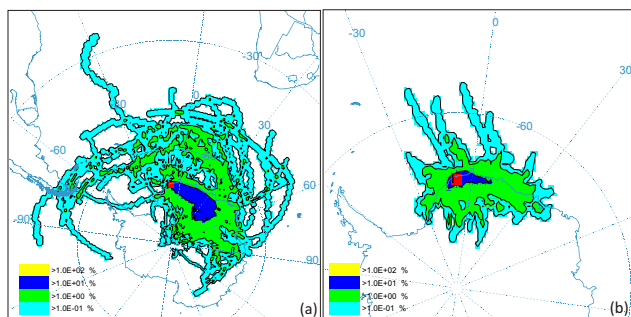


Fig. 6. The 10-day back trajectories for lowest  $^{222}\text{Rn}$  activity concentrations.

a characteristic advection scheme. In addition most of the shown trajectories implied long-range transport. Considering in summary all daily trajectories in conjunction with the NM  $^{222}\text{Rn}$  time series, during summer 10-day backward trajectories related to low  $^{222}\text{Rn}$  events (below 1 SD of the mean, i.e.  $< 0.013 \text{ Bq m}^{-3}$ ,  $N = 139$ ) seem mainly localized at distances less than 1000 km to NM. Corresponding trajectories linked with elevated  $^{222}\text{Rn}$  activity concentrations (1 SD above of the mean, i.e.  $> 0.043 \text{ Bq m}^{-3}$ ,  $N = 188$ ) frequently indicated long-range transport (Fig. 7). Remarkably in this case, a large part of the trajectories move across the Antarctic plateau (Fig. 7a; blue region showing the highest relative number of trajectories intersecting with a  $1^\circ \times 1^\circ$  grid cell), contrary to the case of low  $^{222}\text{Rn}$  conditions (Fig. 7b). Finally, we note that immediate air mass transport from South America was found to be generally rare: less than 5 % of all 10-day backward trajectories eventually originated from this radon source region. Concerning winter, no meaningful differences in the trajectory pattern between high (above 1 SD of the mean, i.e.  $> 0.023 \text{ Bq m}^{-3}$  in this case,  $N = 257$ ) and low (below 1 SD of the mean, i.e.  $< 0.007 \text{ Bq m}^{-3}$ ,  $N = 209$ )  $^{222}\text{Rn}$  activity concentrations were obvious (Fig. 8).



**Fig. 7.** Daily 10-day back trajectories for summer. Shown is the relative (percentage) number of trajectory intersection on a given grid cell (resolution  $1^\circ \times 1^\circ$ ). The left-hand plot (a) presents all 10-day back trajectories for  $^{222}\text{Rn}$  activity concentrations above 1 SD of the mean ( $>0.043 \text{ Bq m}^{-3}$ ,  $N = 188$ ), while on the right (b) the corresponding 10-day back trajectories for  $^{222}\text{Rn}$  activity concentrations below 1 SD of the mean ( $<0.013 \text{ Bq m}^{-3}$ ,  $N = 139$ ) are shown.

In summary, elevated  $^{222}\text{Rn}$  activity concentrations at NM tended to be typically linked with southerly air mass flow from the Antarctic Plateau and especially during winter, to a transiently turbulent (local) PBL. Based on our observations, the role of  $^{222}\text{Rn}$  emissions from ice-free regions in Antarctica could not be assessed, though the fact that  $^{222}\text{Rn}$  levels at NM were comparable to the rocky site DDU cast into doubt a significant contribution of ice-free regions. Surprisingly and in contrast to previous reporting on Antarctic radon (Antarctic Peninsula: Polian et al., 1986 and Pereira, 1990; NM data from 1984 to 1989: Wyputta, 1997), at least for summer  $^{222}\text{Rn}$  levels at NM appeared to be relatively low during stormy conditions, i.e. when NM was governed by northerly passing cyclones. As for winter, a cyclonic impact on  $^{222}\text{Rn}$  levels was not apparent at all.

## 4 Discussion

### 4.1 Seasonal aspects: impact of transport efficiency

Previous measurements indicated that atmospheric  $^{222}\text{Rn}$  activity concentrations decrease distinctly from temperate regions of the Southern Ocean towards Antarctica (Polian et al., 1986, Lambert et al., 1990). Highest mean values were observed on the sub-polar sites Îles Crozet, Îles Kerguelen, and Amsterdam Island (annual mean around  $0.04 \text{ Bq m}^{-3}$ ). At these sites  $^{222}\text{Rn}$  time series were accompanied by a seasonal maximum between May and August (Polian et al., 1986). For coastal Antarctica annual mean  $^{222}\text{Rn}$  activity concentrations measured at Dumont d'Urville (DDU) appeared comparable to NM, but were about a factor of two lower at Mawson. Although the reported  $^{222}\text{Rn}$  seasonality at DDU and Mawson was similar to NM and characterized by a marked maximum during polar day (summer), the seasonal amplitude at Mawson was much lower (Polian et al., 1986;

Lambert et al., 1990). Note, however, that the distinct discrepancy in the summer maximum between DDU and Mawson is not supported by more recent observations from the latter site (Zhang et al., 2011, Fig. 11 therein). At the Antarctic Peninsula (Vernadsky Station,  $65^\circ 15' \text{S}$ ,  $64^\circ 16' \text{W}$ ) the  $^{222}\text{Rn}$  maximum was shifted to April (Ilić et al., 2005). Obviously,  $^{222}\text{Rn}$  seasonality at sub-Antarctic islands showed the exact opposite to those of coastal Antarctica. Lowest  $^{222}\text{Rn}$  levels were reported from the South Pole (typically between  $0.011$  and  $0.015 \text{ Bq m}^{-3}$ ), but here the reported data set was too short to derive an annual cycle (Maenhaut et al., 1979). The different seasonality and higher  $^{222}\text{Rn}$  levels within the temperate zone of the Southern Ocean compared to Antarctica has been explained by (i) a closer proximity to the northern source continents and (ii) efficient long-range transport from these sources by cyclonic activity peaking in the winter season (Polian et al., 1986). For Antarctica, on the other hand, the persistence of the surface inversion layer during polar night prevents down-mixing of air masses from northerly regions and shifts the seasonal maximum towards polar summer (Polian et al., 1986). These assumptions definitely neglected the impact of regional or even nearby oceanic  $^{222}\text{Rn}$  emissions. Model simulations by Heimann et al. (1990) considering merely long-range  $^{222}\text{Rn}$  transport from northerly continents to Antarctica essentially failed in describing the annual  $^{222}\text{Rn}$  cycle observed at DDU.

In discussing the pronounced  $^{222}\text{Rn}$  seasonality at NM, we have first to consider a potential impact of the disequilibrium between  $^{222}\text{Rn}$  and the (measured)  $^{214}\text{Po}$  activity, discussed by Levin et al. (2002), as well as a potential loss of un-attached  $^{222}\text{Rn}$  progeny in the aerosol-based sampling system. The apparent resemblance of the mean  $^{222}\text{Rn}$  seasonality (Fig. 4) with the mean annual cycle of condensation particle (CP) concentrations at NM (Weller et al., 2011a, Fig. 4 therein) suggests such an interference. Unlike the noble gas  $^{222}\text{Rn}$  the metal  $^{214}\text{Po}$  is attached to sub- $\mu\text{m}$  aerosol particles and hence the disequilibrium could be higher at low particle concentrations during winter. To clarify this point, we investigated the relation between CP concentrations and  $^{222}\text{Rn}$  activity concentrations. The result is shown in Fig. 9. We calculated a Pearson correlation coefficient  $r$  to be  $0.213$  ( $r^2 = 0.045$ ;  $N = 42434$ ) for the highest available temporal resolution of the data (3-hour means), and somewhat higher for daily mean values ( $r^2 = 0.076$ ;  $N = 5365$ ). In addition we repeated the correlation analysis with corresponding monthly anomalies of the measured CP concentrations and  $^{222}\text{Rn}$  activity concentrations (for calculation of anomalies see Weller et al., 2011b). No statistically significant correlation ( $r^2 = 0.02$ ,  $p = 0.084$ ;  $N = 206$ ) could be detected in this case. We reason that at most less than about 7.6 % of the  $^{222}\text{Rn}$  variability could be explained by CP concentration variability, excluding a relevant impact of particle number concentrations on observed  $^{222}\text{Rn}$  activity (note that the peak-to-valley ratio of the annual  $^{222}\text{Rn}$  cycle is around a factor of three). In addition we could not find any statistically

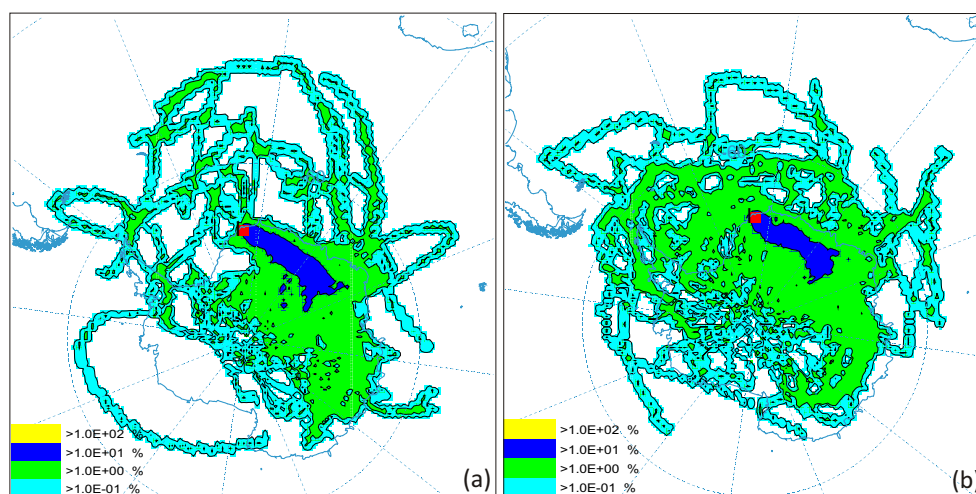


**Fig. 8.** The same presentation as in Fig. 7, but now for winter: (a) all 10-day back trajectories for  $^{222}\text{Rn}$  activity concentrations above 1 SD of the mean ( $>0.023 \text{ Bq m}^{-3}$ ,  $N = 257$ ) and (b) for  $^{222}\text{Rn}$  activity concentrations below 1 SD of the mean ( $<0.007 \text{ Bq m}^{-3}$ ,  $N = 209$ ).

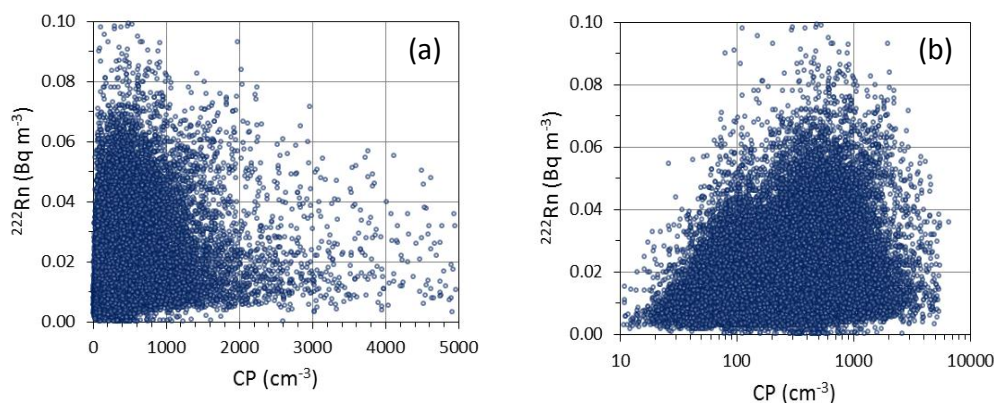


**Fig. 9.** Relation between CP concentrations presented on (a) linear as well as (b) on logarithmic scale and  $^{222}\text{Rn}$  activity concentrations. Data points correspond to 3 h means, i.e. the highest available temporal resolution of the measured  $^{222}\text{Rn}$  activity concentrations. The calculated Pearson correlation coefficient is  $r = 0.213$  ( $r^2 = 0.045$ ;  $N = 42434$ ).

significant impact of potentially aerosol-depleting weather conditions like snow drift, precipitation or (very rare) fog events on observed  $^{222}\text{Rn}$  activity concentrations at NM. Concerning inlet efficiency, test measurements indicate only minor  $^{222}\text{Rn}$  losses, typically within 5–10 %.

Consequently other potential reasons for the observed  $^{222}\text{Rn}$  seasonality have to be examined. With the tentative assumption that in our case a southern hemispheric continent north of Antarctica is the main source region for atmospheric  $^{222}\text{Rn}$ , a comparison with the mean annual cycle of the following tracers and parameters also measured at NM appeared worthwhile and is summarized in Fig. 10: (a) the  $^{222}\text{Rn}$  progeny  $^{210}\text{Pb}$  (Elsässer et al., 2011), (b) the mineral dust tracer Lanthanum (La) for which the main source region is again South America (Weller et al., 2008), (c) the bulk Richardson number as a measure for boundary layer stability, and finally (d) SIE. Obviously, amplitude and narrow

width of the seasonal  $^{222}\text{Rn}$  maximum were clearly outstanding among all the other atmospheric tracers. Only regional SIE showed a strong and narrow minimum coinciding with the  $^{222}\text{Rn}$  maximum (Fig. 10d).

A potential cause of the different seasonality observed for  $^{222}\text{Rn}$  and its progeny  $^{210}\text{Pb}$  could be wet and dry deposition, which is almost irrelevant for the noble gas  $^{222}\text{Rn}$  but crucial for the particle-bound  $^{210}\text{Pb}$  isotope. But from this point of view, it is hard to explain why  $^{210}\text{Pb}$  was apparently much more efficiently depleted during mid-summer (JFM) compared to spring (Figs. 4 and 10a). The situation is different at DDU where  $^{222}\text{Rn}$  and  $^{210}\text{Pb}$  seasonality coincided as expected (Lambert et al., 1990). Similar to  $^{210}\text{Pb}$  the mineral dust tracer La showed at NM a rather broad annual cycle, in contrast to  $^{222}\text{Rn}$  and  $^{210}\text{Pb}$  (Figs. 4, 10a and b). As discussed by Elsässer et al. (2011), the amplitude of La cycle was significantly higher, most probably due to the stronger

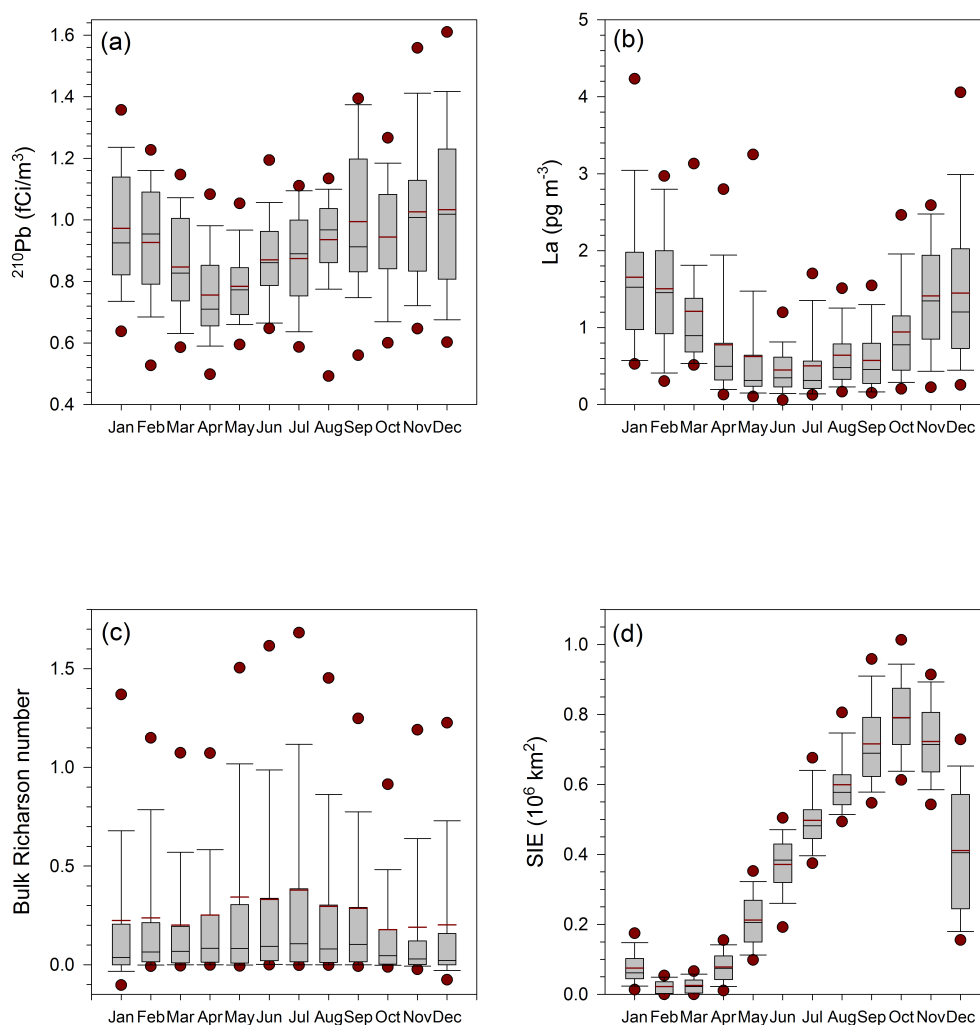


**Fig. 10.** Box plots for the mean seasonality of (a)  $^{210}\text{Pb}$  concentration, (b) La concentration, (c) bulk Richardson number  $Ri_B$  and (d) SIE for the sector  $20^\circ$ – $30^\circ$ . For description of symbols see Fig. 4.

seasonality of the mineral dust source strength and higher atmospheric residence time of  $^{210}\text{Pb}$  compared to the primarily large mineral dust particles (Elsässer et al., 2011). Finally, the seasonality of boundary layer stability estimated by  $Ri_B$  appeared as the less pronounced and most dissimilar compared to  $^{222}\text{Rn}$  (Fig. 10c). Consequently, in terms of source strength and atmospheric transport efficiency we would expect a much broader and less pronounced seasonal  $^{222}\text{Rn}$  maximum at NM provided that South America was the main source region.

#### 4.2 Seasonal aspects: impact of marine emissions and SIE

There are marked similarities between the seasonality of  $^{222}\text{Rn}$  and SIE indicating oceanic  $^{222}\text{Rn}$  emissions as main source. In this case only open water comes into consideration, because the ice shelf itself and also the sea-ice-covered

ocean can be regarded as negligible  $^{222}\text{Rn}$  sources. This source should be dominant during SIE minimum concurrently with the annual  $^{222}\text{Rn}$  summer maximum (Figs. 4 and 10d). Notwithstanding, a statistical analysis based on daily SIE data in  $10^\circ$  longitude resolution along with  $^{222}\text{Rn}$  activity concentrations generally revealed an only weak correlation. Regarding summer, the correlation between both parameters, calculated by a bivariate regression considering the uncertainties of both variables (Cantrell, 2008), was actually highest for the SIE sector  $20^\circ$  E to  $30^\circ$  E whereby about 8.1% ( $p < 10^{-20}$ ) of the  $^{222}\text{Rn}$  variability could be explained by SIE variability (Fig. 11). For winter, we did not detect any significant correlation. Finally, we found an only minor impact of nearby oceanic  $^{222}\text{Rn}$  emissions (and consequentially local SIE variability): During summer, we measured definitely lower  $^{222}\text{Rn}$  activity concentrations under northerly flow conditions, i.e. advection from the open water ahead of NM (regarding daily means:  $0.0231 \text{ Bq m}^{-3}$  for northerly

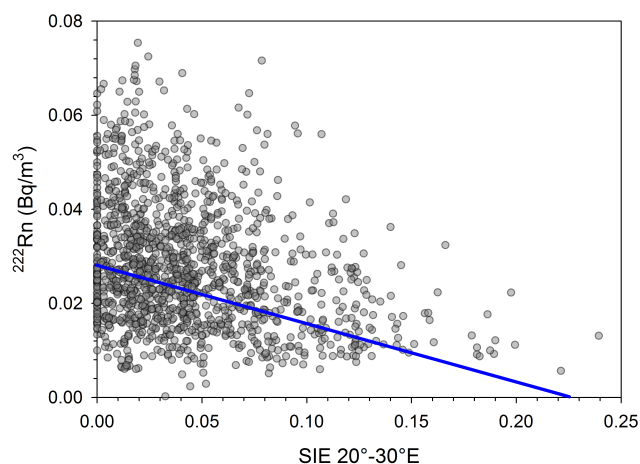


**Fig. 11.** Correlation between  $^{222}\text{Rn}$  activity and SIE (unit:  $10^6 \text{ km}^2$ ) between  $20^\circ\text{E}$  and  $30^\circ\text{E}$  for summer (JFM) based on respecting daily mean values. Regression (blue line) calculated by the Williamson–York method (Cantrell, 2008) with slope  $= -(0.124 \pm 0.028) \times 10^{-6} \text{ Bq m}^{-3} \text{ km}^{-2}$ , intercept  $= (0.028 \pm 0.001) \text{ Bq m}^{-3}$ .

wind direction between  $300^\circ$  and  $60^\circ$ ,  $N = 293$  cases, compared to  $0.0286 \text{ Bq m}^{-3}$  for remaining wind directions between  $60^\circ$  and  $300^\circ$ ,  $N = 9460$ ,  $p < 10^{-7}$ ). Hence a significant influence of SIE modulated oceanic  $^{222}\text{Rn}$  emissions appeared arguable.

Nevertheless, considering and balancing all findings presented above, we tentatively suggest the regional SIE variability as a significant driver of the observed  $^{222}\text{Rn}$  seasonality. The moderate correlation between both parameters appears not so surprising, keeping in mind that oceanic  $^{222}\text{Rn}$  emission strength is (apart from SIE) highly dependent on surface wind velocity (Schery and Huang, 2004; Taguchi et al., 2013). Source strength and also transport efficiency associated with air mass history determined  $^{222}\text{Rn}$  activity concentrations eventually measured at NM. The impact of these different processes may have blurred an inherently more pronounced correlation with SIE data. Most probably the main oceanic source regions were some  $1000 \text{ km}$  away from NM, as supported by trajectory analyses which indicate as well a main transport route via the Antarctic continent (Fig. 7a). In addition, the long transport routes indicated in Fig. 7a imply high wind velocities and efficient sea–air exchange processes. The exceptionally low  $^{222}\text{Rn}$  activity concentrations measured under advection from open water ahead of NM may be a consequence of the generally very low wind velocities ( $4 \pm 3 \text{ m s}^{-1}$ ) and hence minimized sea–air exchange under these conditions.

## 5 Conclusions

$^{222}\text{Rn}$  activity levels measured at NM were in principle consistent with those observed at Cape Grim provided that the latter site was governed by advection of clean marine air masses. Following the arguments of Zahorowski et al. (2013), in such air masses  $^{222}\text{Rn}$  levels should be determined by marine emissions. This finding motivated the attractive hypothesis that also  $^{222}\text{Rn}$  activity concentrations at NM and in particular their distinct seasonality may be largely caused by marine emissions and inherently linked with the annual cycle of SIE. In addition, sporadic radon storms should have been caused by long-range transport of continental air masses from South America. Actually, based on our present evaluation, a more complicated and somewhat ambiguous general view emerged. Although we could not properly assess the contribution of oceanic  $^{222}\text{Rn}$  emissions to the observed  $^{222}\text{Rn}$  activity concentrations at NM, we can state that the marine  $^{222}\text{Rn}$  source and the impact of SIE should be of significant importance in particular concerning the distinct seasonal maximum in February coinciding with the regional SIE minimum. Regarding trajectory analyses and local meteorology, there was a distinct difference during summer in air mass characteristics between high and low  $^{222}\text{Rn}$  activity concentrations: high  $^{222}\text{Rn}$  activity concentrations were generally associated with long-range transport, while advection during low  $^{222}\text{Rn}$  activity concentrations was more regionally confined (less than  $1000 \text{ km}$  ambit). Long-range transport is typically associated with high wind velocities promoting sea–air exchange processes. Furthermore, air masses with high  $^{222}\text{Rn}$  activity concentrations seem to arrive at NM preferentially via the Antarctic plateau, probably after down-mixing of free tropospheric air masses. At first sight, these latter findings seem also to be consistent with the previously raised assumption that  $^{222}\text{Rn}$  activity at coastal NM should be governed by long-range air mass transport from South America and modulated by the efficiency of downward mixing into the PBL over Antarctica (Polian et al., 1986). Nevertheless, in our case the distinct seasonality of  $^{222}\text{Rn}$  levels (and especially the divergent annual cycle of  $^{210}\text{Pb}$  concentrations) could not satisfactorily be explained with it. Lastly, we found that high  $^{222}\text{Rn}$  activity concentrations were usually not associated with cyclonic activities and, on the whole, the impact of immediate long-range transport from the South American continent emerged as marginal. Consequently, at least for NM but most probably also for other Antarctic sites, the usage of  $^{222}\text{Rn}$  activity concentrations to assess air mass history remains ambiguous. To clarify this crucial point, there is a need for extensive measurements of vertical  $^{222}\text{Rn}$  profiles above Antarctica and the Southern Ocean, particularly under different general weather situations. Finally, one has to keep in mind that the validity of the presented backward trajectory analyses is somewhat limited. The use of more sophisticated dispersion models considering all available Antarctic  $^{222}\text{Rn}$  records should

significantly improve our knowledge about processes governing the spatial and temporal variability of the Antarctic  $^{222}\text{Rn}$  inventory.

*Acknowledgements.* The authors would like to thank the many technicians and scientists of the Neumayer overwintering crews, whose outstanding commitment has enabled the achievement of continuous, high quality aerosol and trace gas records since 1982. Special thanks go to Holger Schmithüsen and Gert König-Langlo for their effort in compiling meteorological data for our purpose. We are thankful to NOAA Air Resources Laboratory for having made available the HYSPLIT trajectory calculation program as well as all input data files used. We also acknowledge partial funding of the initial phase of the air chemical NM Observatory programme by the German Science Foundation (DFG) as well as financial support obtained within the European Community STEP programme within the project Polar Atmospheric Chemistry.

Edited by: M. Heimann

## References

- Anderson, P. S. and Neff, W. D.: Boundary layer physics over snow and ice, *Atmos. Chem. Phys.*, 8, 3563–3582, doi:10.5194/acp-8-3563-2008, 2008.
- Cantrell, C. A.: Technical Note: Review of methods for linear least-squares fitting of data and application to atmospheric chemistry problems, *Atmos. Chem. Phys.*, 8, 5477–5487, doi:10.5194/acp-8-5477-2008, 2008.
- Caughey, S. J., Wyngaard, J. C., and Kaimal, J. C.: Turbulence in the Evolving Stable Boundary Layer, *J. Atmos. Sci.*, 6, 1041–1052, 1979.
- Elsässer, C., Wagenbach, D., Weller, R., Auer, M., Wallner, A., and Christl, M.: Continuous 25-years aerosol records at coastal Antarctica: Part 2: variability of the radionuclides  $^7\text{Be}$ ,  $^{10}\text{Be}$  and  $^{210}\text{Pb}$ , *Tellus*, 63B, 920–934, doi:10.1111/j.1600-0889.2011.00543.x, 2011.
- Fernando, H. J. S. and Weil, J. C.: Whither the Stable Boundary Layer? A Shift in the Research Agenda, *B. Am. Meteor. Soc.*, 91, 1475–1484, doi:10.1175/2010BAMS2770.1, 2010.
- Handorf, D.: Zur Parametrisierung der stabilen atmosphärischen Grenzschicht über einem antarktischen Schelfeis, in *Reports on Polar and Marine Research*, 204, edited by: Riemann, F., Alfred-Wegener-Inst. for Polar and Marine Res., Bremerhaven, 1996.
- Harris, J. M., Draxler, R. R., and Oltmans, S. J.: Trajectory model sensitivity to differences in input data and vertical transport method, *J. Geophys. Res.*, 110, D14109, doi:10.1029/2004JD005750, 2005.
- Harrison, R. G. and Carslaw, K. S.: Ion-aerosol-cloud processes in the lower atmosphere, *Rev. Geophys.*, 41, 1012, doi:10.1029/2002RG000114, 2003.
- Heimann, M., Monfray, P., and Polian, G.: Modeling the long-range transport of  $^{222}\text{Rn}$  to subantarctic and Antarctic areas, *Tellus*, 42B, 83–99, 1990.
- Hirsch, R. M., Slack, J. R., and Smith, R. A.: Techniques of trend analysis for monthly water quality data, *Water Resour. Res.* 18, 107–121, 1982.
- Hirsikko, A., Nieminen, T., Gagné, S., Lehtipalo, K., Manninen, H. E., Ehn, M., Hörrak, U., Kerminen, V.-M., Laakso, L., McMurry, P. H., Mirme, A., Mirme, S., Petäjä, T., Tammet, H., Vakkari, V., Vana, M., and Kulmala, M.: Atmospheric ions and nucleation: a review of observations, *Atmos. Chem. Phys.*, 11, 767–798, doi:10.5194/acp-11-767-2011, 2011.
- Ilić, R., Rusov, V. D., Pavlovych, V. N., Vaschenko, V. M., Hanžič, L., Bondarchuk, Y. A.: Radon in Antarctica, *Radiat. Meas.*, 40, 415–422, 2005.
- Jacob, D. J., Prather, M. J., Rasch, P. J., Shia, R.-L., Balkanski, Y. J., Beagle, S. R., Bergmann, D. J., Blackshear, W. T., Brown, M., Chiba, M., Chipperfield, M. P., de Grandpré, J., Dignon, J. E., Feichter, J., Genthon, C., Grose, W. L., Kasibhatla, P. S., Köhler, I., Kritz, M. A., Law, K., Penner, J. E., Ramonet, M., Reeves, C. E., Rotman, D. A., Stockwell, D. Z., Van Velthoven, P. F. J., Verver, G., Wild, O., Yang, H., and Zimmermann, P.: Evaluation and intercomparison of global atmospheric transport models using  $^{222}\text{Rn}$  and other short-lived tracers, *J. Geophys. Res.*, 102, 5953–5970, doi:10.1029/96JD02955, 1997.
- Jones, A. E., Anderson, P. S., Wolff, E. W., Roscoe, H. K., Marshall, G. J., Richter, A., Brough, N., and Colwell, S. R.: Vertical structure of Antarctic tropospheric ozone depletion events: characteristics and broader implications, *Atmos. Chem. Phys.*, 10, 7775–7794, doi:10.5194/acp-10-7775-2010, 2010.
- Karstens, U., Schmithüsen, D., Schwingshackl, C., and Levin, I.: A process-based  $^{222}\text{Rn}$  flux map for Europe and its verification by long-term observations, to be submitted to *Atmos. Chem. Phys. Discuss.*, 2014.
- König-Langlo, G., King, J. C., and Pettré, P.: Climatology of the three coastal Antarctic stations Dumont d'Urville, Neumayer and Halley, *J. Geophys. Res.*, 103, 10935–10946, 1998.
- Lambert, G., Ardouin, B., and Sanak, J.: Atmospheric transport of trace elements toward Antarctica, *Tellus*, 42B, 76–82, 1990.
- Law, R. M., Steele, L. P., Krummel, P. B., and Zahorowski, W.: Synoptic variation in atmospheric  $\text{CO}_2$  at Cape Grim: a model intercomparison, *Tellus*, 62B, 810–820, doi:10.1111/j.1600-0889.2010.00470.x, 2010.
- Levin, I., Born, M., Cuntz, M., Langendörfer, U., Mantsch, S., Naegler, T., Schmidt, M., Varlagin, A., Verclas, S., and Wagenbach, D.: Observations of atmospheric variability and soil exhalation rate of radon-222 at a Russian forest site, *Tellus*, 54B, 462–475, 2002.
- Liu, S. C., McAfee, J. R., and Cicerone, R. J.: Radon 222 and tropospheric Vertical Transport, *J. Geophys. Res.*, 89, 7291–7297, 1984.
- Maenhaut, W., Zoller, W. H., and Coles, D. G.: Radionuclides in the South Pole Atmosphere, *J. Geophys. Res.*, 84, 3131–3138, 1979.
- Mauritsen, T. and Svensson, G.: Observations of stably stratified shear-driven atmospheric turbulence at low and high Richardson numbers, *J. Atmos. Sci.*, 64, 645–655, 2007.
- Nazaroff, W. W.: Radon Transport From Soil to Air, *Rev. Geophys.*, 30, 137–160, 1992.
- Pereira, E. B.: Radon-222 time series measurements in the Antarctic peninsula (1986–1987), *Tellus*, 42B, 39–45, 1990.
- Polian, G., Lambert, G., Ardouin, B., and Jegou, A.: Long-range transport of continental radon in subantarctic and antarctic areas, *Tellus*, 38B, 178–189, 1986.

- Porstendörfer, J.: Properties and behaviour of Radon and Thoron and their decay products in the air, *J. Aerosol Sci.*, 25, 219–263, 1994.
- Schery, S. D. and Huang, S.: An estimate of the global distribution of radon emissions from the ocean, *Geophys. Res. Lett.*, 31, L19104, doi:10.1029/2004GL021051, 2004.
- Slemr, F., Brunke, E.-G., Whittlestone, S., Zahorowski, W., Ebinghaus, R., Kock, H.H., and Labuschagne, C.:  $^{222}\text{Rn}$ -calibrated mercury fluxes from terrestrial surface of southern Africa, *Atmos. Chem. Phys.*, 13, 6421–6428, doi:10.5194/acp-13-6421-2013, 2013.
- Stohl, A.: Computation, accuracy and applications of trajectories: a review and bibliography, *Atmos. Environ.*, 32, 947–966, 1998.
- Stull, R. B.: *An Introduction to Boundary Layer Meteorology*, Kluwer Academic Publishers, Dordrecht, Dordrecht, 175–180, 1988.
- Taguchi, S., Tasaka, S., Matsubara, M., Osada, K., Yokoi, T., and Yamanouchi, T.: Air-sea gas transfer rate for the Southern Ocean inferred from  $^{222}\text{Rn}$  concentrations in maritime air and a global atmospheric transport model, *J. Geophys. Res. Atmos.*, 118, 7606–7616, doi:10.1002/jgrd.50594, 2013.
- Wagenbach, D., Görlach, U., Moser, K., and Münnich, K. O.: Coastal Antarctic aerosol: the seasonal pattern of its chemical composition and radionuclide content, *Tellus*, 40B, 423–436, 1988.
- Weller, R., Wöltjen, J., Piel, C., Resenberg, R., Wagenbach, D., König-Langlo, G., and Kriews, M.: Seasonal variability of crustal and marine trace elements in the aerosol at Neumayer station, Antarctica, *Tellus*, 60B, 742–752, doi:10.1111/j.1600-0889.2008.00372.x, 2008.
- Weller, R., Minikin, A., Wagenbach, D., and Dreiling, V.: Characterization of the inter-annual, seasonal, and diurnal variations of condensation particle concentrations at Neumayer, Antarctica, *Atmos. Chem. Phys.*, 11, 13243–13257, doi:10.5194/acp-11-13243-2011, 2011a.
- Weller, R., Wagenbach, D., Legrand, M., Elsässer, C., Tian-Kunze, X., and König-Langlo, G.: Continuous 25-years aerosol records at coastal Antarctica – 1: inter-annual variability of ionic compounds and links to climate indices, *Tellus*, 63B, 901–919, doi:10.1111/j.1600-0889.2011.00542.x, 2011b.
- Wilkening, M. H. and Clements, W. E.: Radon 222 from the Ocean Surface, *J. Geophys. Res.*, 80, 3828–3830, 1975.
- Wyputta, U.: On the transport of trace elements into Antarctica using measurements at the Georg-von-Neumayer station, *Tellus*, 49B, 93–111, 1997.
- Zahorowski, W., Griffiths, A. D., Chambers, S. D., Williams, A. G., Law, R. M., Crawford, J., and Werczynski, S.: Constraining annual and seasonal radon-222 flux density from the Southern Ocean using radon-222 concentrations in the boundary layer at Cape Grim, *Tellus*, 65B, 1962, doi:10.3402/tellusb.v65i0.19622, 2013.
- Zhang, K., Feichter, J., Kazil, J., Wan, H., Zhuo, W., Griffiths, A. D., Sartorius, H., Zahorowski, W., Ramonet, M., Schmidt, M., Yver, C., Neubert, R. E. M., and Brunke, E.-G.: Radon activity in the lower troposphere and its impact on ionization rate: a global estimate using different radon emissions, *Atmos. Chem. Phys.*, 11, 7817–7838, doi:10.5194/acp-11-7817-2011, 2011.